Available online at www.sciencedirect.com
ScienceDirect
Journal of Sound and Vibration 321 (2009) 319–341
JOURNAL OF SOUND AND VIBRATION
www.elsevier.com/locate/jsvi

Nonlinear dynamics of a friction-limited drive: Application to a chain continuously variable transmission (CVT) system

Nilabh Srivastava[a,*], Imtiaz Haque[b]

[a]Department of Mechanical Engineering, University of North Carolina at Charlotte, DCH 355, Charlotte, NC 28269, USA
[b]Department of Mechanical Engineering, Clemson University, EIB 106, Clemson, SC 29634, USA

Received 22 May 2007; received in revised form 17 September 2008; accepted 19 September 2008
Handling Editor: S. Bolton
Available online 6 November 2008

Abstract

Over the past two decades, extensive research has been conducted on developing vehicle transmissions that meet the goals of reduced exhaust emissions and increased vehicle efficiency. A continuously variable transmission is an emerging automotive transmission technology that offers a continuum of gear ratios between desired limits. A chain CVT is a friction-limited drive whose dynamic performance and torque capacity rely significantly on the friction characteristic of the contact patch between the chain and the pulley. Although a CVT helps to maximize the vehicle fuel economy, its complete potential has not been accomplished in a mass-production vehicle. The present research focuses on developing models to analyze friction-induced nonlinear dynamics of a chain CVT drive and identify possible mechanisms that cause degradation of the overall dynamic performance by inducing chaos and self-sustained vibrations in the system. Two different mathematical models of friction, which characterize different operating or loading conditions, are embedded into a detailed planar multibody model of chain CVT in order to capture the various friction-induced effects in the system. Tools such as stick–slip oscillator dynamics, Lyapunov exponents, phase-space reconstruction, and recurrence plotting are incorporated to characterize the nonlinear dynamics of such a friction-limited system. The mathematical models, the computational scheme, and the results corresponding to different loading scenarios are discussed. The results discuss the influence of friction characteristics on the nonlinear dynamics and torque transmitting capacity of a chain CVT drive.

1. Introduction

Over the last few decades, vehicles have been increasingly facing stringent performance, emissions, and fuel economy standards driven by regulatory and market forces. Automobile energy consumption is a key element in the current debate on global warming. The global need for improved fuel economy and reduced emissions has fostered research advancements in engine and transmission designs. Lately, continuously variable transmissions (CVTs) have aroused a great deal of interest in the automotive sector due to the potential of lower emissions and better performance. A CVT is an emerging automotive transmission technology that offers an infinite number of gear ratios between two limits, which consequently enhances the vehicle fuel economy and performance by

*Corresponding author. Tel.: +1 704 687 7499; fax: +1 704 687 8345.
E-mail addresses: nsrivast@uncc.edu, nilsri77@yahoo.com (N. Srivastava).

0022-460X/$ - see front matter © 2008 Elsevier Ltd. All rights reserved.
doi:10.1016/j.jsv.2008.09.045

Nomenclature

a	starting coefficient of friction between chain and pulley ($\sim$0.003)
(a_{cx}, a_{cy})	linear acceleration of the center of mass of a link
$1/b,\kappa$	rate of growth of friction coefficient, μ
d	embedding delay
$\mathbf{h}$	forcing vector containing contributions from active forces/torques and other gyroscopic terms
I_c	moment of inertia of a chain link about its center of mass
J_p	pulley rotational inertia
k, p	stiffness and damping parameters of the interconnecting force element
m	mass of a chain link; embedding dimension
$\mathbf{M}$	mass matrix (assembled)
r, r'	link pitch radius on driver and driven pulleys, respectively
u	axial width variation due to pulley flexibility
v_{rel}	relative velocity between the contacting surfaces
(x_c, y_c)	coordinates of the center of mass of a link
z	local distance between the pulley sheaves
β_0	half-sheave angle of the non-deformed pulley
β	half-sheave angle of the deformed pulley
γ	sliding angle
Δ	amplitude of the sheave angle sinusoid
ζ	angular location of a link over the pulley wrap
θ	rotational degree-of-freedom of a link
θ_c	angular location of the center of pulley wedge expansion
$\boldsymbol{\lambda}_{\mathbf{N}}$, $\mathbf{N}$	normal force between a chain link and a pulley
$\boldsymbol{\lambda}_{\mathbf{T}}$	force during the sticking phase of a contact
μ	coefficient of friction between a link and the pulley
μ_0	coefficient of kinetic friction between a link and the pulley
σ	parameter related to the ratio of the coefficients of static and kinetic friction
τ	torque transmitted by the driver pulley
φ	pulley rotational degree-of-freedom
χ	Stribeck-effect/lubrication parameter
$\dot{g}$	relative velocity between a link and the pulley in the sliding plane
$\dot{g}_r$	radial component of the relative velocity between a link and the pulley
$\aleph$	slope parameter for the smoothened signum function model
$\overline{\lambda}$	Lyapunov exponent of a dynamical system
δs	separation distance between two nearby points in phase space
CVT	continuously variable transmission

allowing better matching of the engine operating conditions to the variable driving scenarios. Today several auto manufacturers such as Honda, Toyota, Ford, Nissan, etc., are already keen on exploiting the various advantages of a CVT (especially belt, chain, toroidal types) in a real production vehicle. In spite of the several advantages proposed by a CVT system, its complete potential, in terms of the mass-production and market penetration of CVT-equipped vehicles, has not been realized so far. In order to achieve lower emissions and better performance, it is necessary to understand the various complex dynamic interactions occurring in a CVT system in detail so that efficient controllers could be designed to overcome the existing losses and enhance vehicle fuel economy.

A chain CVT consists of two variable diameter pulleys kept at a fixed distance apart and connected to each other by a chain. Fig. 1 depicts the chain structure and the basic configuration of a chain CVT drive. A rocker-pin chain consists of plates and rocker pins, as depicted in the figure. All plates and pins transmit tractive power. One of the sheaves on each pulley is movable. So, the chain is capable of exhibiting both radial and tangential motions depending on the torque loading conditions and the axial forces applied to the pulley sheaves. Moreover, the contact forces between the rocker pins and the pulleys are discretely distributed. Consequently, impact-related vibrations occur as chain links enter and leave the pulley. These excitation mechanisms, which are related to the polygonal action of chain links, significantly influence the performance of a chain CVT drive. The pulley on the engine side is called the driver pulley and the one on the final drive side is called the driven pulley.

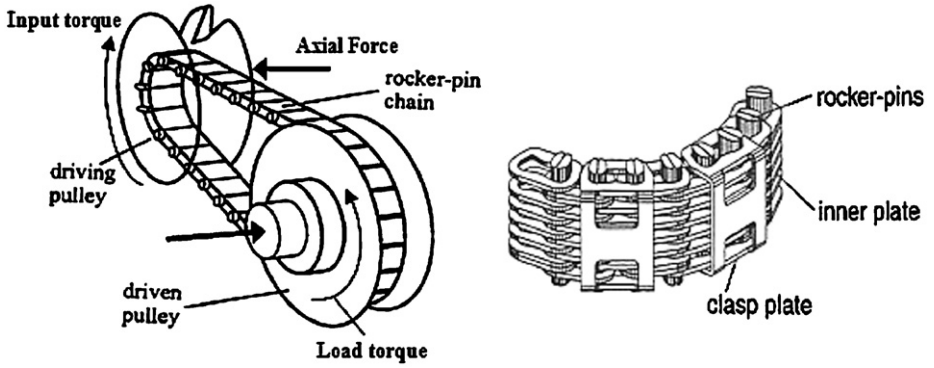

Fig. 1. Chain CVT configuration and chain link structure.

A chain CVT falls under the category of friction-limited drives as its dynamic performance and torque capacity rely significantly on the friction characteristic of the contact patch between the chain and the pulley. Although the friction characteristic of the contacting surface inevitably plays a crucial role on CVT's performance, literature pertaining to the influence of friction on the dynamics of a CVT system is scarce. Almost all models, barring a few, mentioned in literature use Coulomb friction theory to model friction between the contacting surfaces of a CVT. However, depending on different operating or loading conditions and design configurations, the friction characteristic of the contacting surface may vary. For instance, in a fully lubricated CVT, the friction characteristic of the contacting surface may bear a resemblance to the Stribeck curve [1] rather than to a continuous Coulomb characteristic. Moreover, very high forces in the contact zone may further lead to the conditions of elasto-plastic-hydrodynamic lubrication, which may yield a different friction characteristic. Since the friction characteristic of the contact patch may vary in accordance with the loading and design configurations, it is crucial to understand its influence on the dynamic performance of a CVT system.

Srnik and Pfeiffer [2,3] studied the dynamic behavior of a CVT chain drive for high torque applications. They developed a planar model of chain CVT with 3D contact between a chain link and the pulley. Their work dealt with multibody formalisms and finite element modeling. Sedlmayr et al. [4,5] extended the previous work done by Srnik et al. [2] to include the effects of spatial orientation on the dynamics of CVT chain drives. The authors modeled the links and the pulleys as elastic bodies and also included pulley misalignment effects. Sattler [6] analyzed the mechanics of metal chain and V-belt considering both longitudinal and transverse stiffness of the chain and the belt, misalignment and deformation of the pulleys. The pulley deformation was modeled using a standard finite-element analysis. The pulley was assumed to deform in two ways, pure axial deformation and a skew deformation. The model was also used to study efficiency aspects of belt and chain CVTs. Tenberge [7] developed a fast computational algorithm to compute the dynamic indicators of a chain CVT from a mathematical model which included deformations, loadings, and other inertial effects at constant and variable speed ratios. Srivastava and Haque [8–12] developed a planar multibody model of a chain CVT and investigated the influence of clearance and friction on the dynamic performance indices of chain CVT drives for high torque applications. They observed that clearance and friction parameters drastically influenced the performance of a CVT system, and could even render the operation perilous by inducing chaos or irregular behavior in the system. However, their work did not include any mathematical analysis needed to understand and capture friction-induced chaos in a CVT system.

A few authors have also investigated and reported the influence of friction characteristics on the performance of a metal belt CVT. A belt CVT, like a chain CVT, is a friction-limited drive; however, the contact force between the belt and the pulley has almost smooth distribution over the pulley wrap unlike in a chain CVT. Lebrecht, Pfeiffer and Ulbrich [13] analyzed self-induced vibrations in a metal pushing V-belt CVT by using highly simplified friction models. It was shown that the certain friction characteristics, especially those having negative gradient with respect to relative velocity, could induce self-excited vibrations in the belt. The friction characteristic and the elasticity of the pulley sheaves also determined the working area where vibrations occurred. Micklem et al. [14] incorporated the elastohydrodynamic lubrication theory to model

friction between the metal V-belt and the pulley and also studied transmission losses due to the wedging action of the belt. Carbone et al. [15] developed a theoretical model of a metal pushing V-belt to understand the transient dynamics of a belt CVT during rapid speed-ratio variations and used two friction models, namely a Coulomb friction model and a visco-plastic friction model, to describe friction between the belt and the pulley and to accurately predict the shifting dynamics during slow and fast maneuvers. Srivastava and Haque [16–20] developed a detailed transient dynamic model of a metal pushing V-belt CVT to evaluate the dynamic performance indices of the belt CVT system under the influence of pulley flexibility and varying friction characteristics of the belt-pulley contact zone. Two different mathematical models of friction were incorporated to describe friction between the belt element and the pulley. These friction models were able to capture effects due to kinetic friction, stiction, and lubricated contact conditions. The authors reported a comparative study on the dynamic performance of a metal V-belt CVT under the influence of these friction models. However, nonlinear phenomena like self-excited vibrations and chaos associated with friction in a belt CVT system were not reported in their work.

To the best of author's knowledge, literature pertaining to the identification of friction-induced nonlinear phenomena and chaos in a CVT system is scarce. It has been briefly reported [8,10,12,13] in literature that certain friction characteristics induce self-excited vibrations or irregular behavior in the CVT system. However, it is not clear whether such phenomenon is an artifact of the friction model or the real behavior of the system. Hence, it is necessary to study the influence of different friction characteristics on the dynamic performance of a CVT system.

The research reported in this paper focuses on the development of a detailed dynamic model of a chain CVT using multibody formalisms. The chain CVT is modeled as a multibody system in order to accurately capture the dynamics arising from the impact and polygonal action of the chain links. The chain CVT model is developed using Pfeiffer and Glocker's theory [21] on multibody dynamics with unilateral contacts. Since it is experimentally cumbersome to measure the exact friction characteristic of the contacting surfaces in a CVT system, different literature-based mathematical models of friction are incorporated in this transient-dynamic CVT model in order to gain insight into the influence of friction on the dynamic performance of a CVT. The goal is to understand friction-induced nonlinear dynamic behavior of a chain CVT drive as the chain links traverse the contacting arcs over the driver and driven pulleys and also to evaluate the system performance under the influence of different contact-zone friction characteristics. The models developed by the author in their previous work [8–12] are further exploited by incorporating the tools of nonlinear dynamics to identify interesting friction-induced chaotic phenomenon in a chain CVT drive under high input-low load conditions. It is important to note that although an exact knowledge of the friction characteristic in a CVT system can only be obtained by conducting experiments on a real production CVT, these mathematical models give profound insight into the probable behavior of a CVT under different operating conditions. This knowledge could be further exploited to design more efficient controllers and identify various loss mechanisms in a CVT system. The modeling analysis and the results corresponding to the chain CVT model are discussed in detail in the subsequent sections.

2. Modeling of a chain CVT

As depicted in Fig. 1, a chain CVT consists of two variable diameter pulleys connected to each other by a chain. The system is subjected to an input torque on the driver pulley and a resisting load torque on the driven pulley. The model development and analysis includes the following assumptions:

(1) The pulleys do not have any misalignment between them.
(2) The chain links are rigid.
(3) The interactions between the rocker pins of neighboring links and between a rocker pin and a plate can all be accounted for by modeling the chain link as a planar rigid body.
(4) Negligible out-of-plane interaction of chain links.
(5) Bending and torsional stiffness of the chain links are neglected.

The modeling of various components of a chain-drive CVT is discussed subsequently.

2.1. Model of chain links

The chain links in the chain CVT are modeled as kinematically decoupled planar rigid bodies which are connected to each other by force elements. Each chain link represents a rigid body with 3-degrees-of-freedom (dof) in a plane (i.e. (x_c, y_c, θ)): two translations of the center of mass of the link and one rotation about an axis passing through the link's center of mass. The force elements take into account the elasticity and damping of the links and joints. In addition to these interconnecting forces, the links also experience contact forces in normal and tangential directions whenever they come in contact with the pulley sheaves. The chain in the CVT is modeled link by link to account for its discrete structure. Figs. 2 and 3 illustrate the free-body diagram of a chain link.

It is to be noted that in Fig. 2, the dotted arrows represent the forces (f_x and f_y), which only arise when a chain link comes in contact with the pulley sheave. Using Newton–Euler formulation [8–12] and the Theory of Unilateral Contacts [2,21], the equation of motion for all links under unilateral contact conditions with the pulleys can be written as

$$\mathbf{M}\ddot{\mathbf{q}} - \mathbf{h} - (\mathbf{W_N} + \mathbf{W_S}\hat{\boldsymbol{\mu}}_\mathbf{S}|\mathbf{W_T})\begin{pmatrix}\boldsymbol{\lambda}_\mathbf{N}\\ \boldsymbol{\lambda}_\mathbf{T}\end{pmatrix} = \mathbf{0},$$

where

$$\hat{\boldsymbol{\mu}}_\mathbf{S} = \{-\mu_i(\dot{g}_i)\,\mathrm{sign}(\dot{g}_i)\}. \tag{1}$$

$\boldsymbol{\lambda}_\mathbf{N}$, $\boldsymbol{\lambda}_\mathbf{T}$ are the normal and the sticking constraint forces of the links that are in contact with the pulley and $\dot{g}_i$ is the relative velocity between a link, i, and the pulley in the sliding plane (refer to Fig. 5). $\mathbf{W_N}$ represents a matrix with coefficients of relative acceleration (in the normal direction) between the links and the pulleys in the configuration space. $\mathbf{W_S}$ represents a matrix with coefficients of relative acceleration (in the slip direction) between the links and the pulleys in the configuration space when the links are slipping on the pulley sheave, whereas $\mathbf{W_T}$ represents a matrix with coefficients of relative acceleration (in the slip direction) between the links and the pulleys in the configuration space when the links are sticking to the pulley sheaves. It is to be noted that these relative velocities and accelerations are computed at the points where the links contact the pulleys.

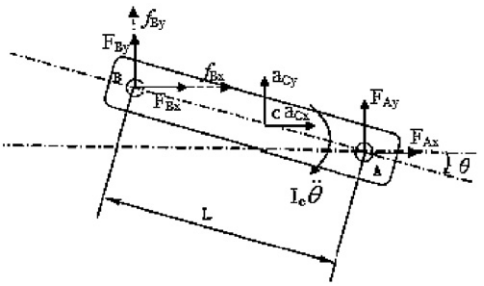

Fig. 2. Free body diagram of a chain link.

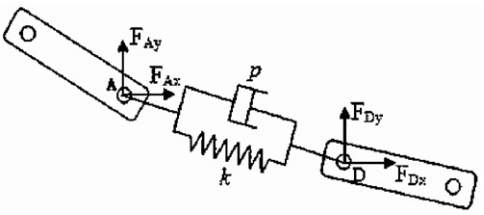

Fig. 3. Free body diagram of chain link interaction.

2.2. Model of pulleys

Each pulley is modeled as a rigid body with 1-dof i.e. the rotational dof (φ). A pulley is loaded not only with the frictional and normal forces between the rocker pins of the links and the pulley, but also with external moments. An input torque is applied to the driver pulley and a load torque on the driven pulley. Similar to Eq. (1), the equation of motion of a pulley under unilateral contact conditions with the links over its contacting arc is given by

$$J_P\ddot{\varphi} = h_P - (\mathbf{W_{Np}} + \mathbf{W_{Sp}}\hat{\boldsymbol{\mu}}_S|\mathbf{W_{Tp}})\begin{pmatrix}\boldsymbol{\lambda}_{\mathbf{Np}}\\ \boldsymbol{\lambda}_{\mathbf{Tp}}\end{pmatrix}. \tag{2}$$

The term, h_P, accounts for the moment contributions from the input and load torques on the pulleys. The terms, $\mathbf{W_{Np}}$, $\mathbf{W_{Sp}}$ and $\mathbf{W_{Tp}}$ are analogous to the terms, $\mathbf{W_N}$, $\mathbf{W_S}$ and $\mathbf{W_T}$ in Eq. (1). It is to be noted that the contact forces exerted on the pulleys would be equal and opposite of the contact forces exerted on the links i.e. $\boldsymbol{\lambda}_{\mathbf{Np}} = -\boldsymbol{\lambda}_{\mathbf{N}}$, $\boldsymbol{\lambda}_{\mathbf{Tp}} = -\boldsymbol{\lambda}_{\mathbf{T}}$.

Since it has been observed [2,4,8–12,19,20,22–24] that the variation of local groove width caused by the elastic deformation of the pulleys significantly influences the thrust ratio and slip behavior of a belt/chain CVT, simple trigonometric functions (as outlined in Refs. [8–12,19,20,23,24]) are used to describe the varying pulley groove angle and the local elastic axial deformations of the pulley sheaves. Fig. 4 depicts the model for pulley deformation. The following equations describe pulley deformation effects in Fig. 4:

$$\beta = \beta_0 + \frac{\Delta}{2}\sin\left(\zeta - \theta_c + \frac{\pi}{2}\right). \tag{3}$$

Using this approximation for the sheave-angle deformation, the pitch radius of a chain link in the deformed pulley sheave can be easily computed. The amplitude of the variation Δ in the pulley groove angle is always much smaller than unity, however, it is not constant during speed-ratio changing phases due to variations in the pulley axial (clamping) forces. Sferra et al. [24] proposed the following approximate correlations for the amplitude variation Δ and the center of pulley wedge expansion θ_c in terms of the transmitted torque τ, and the chain pitch radius on driver and driven pulleys, r and r', respectively,

$$\Delta = \frac{0.00045}{\left(\frac{r}{r'}\right)^{0.55}},$$

$$\theta_c = \frac{\pi}{3}\frac{r}{r'} + \frac{23\pi}{180}. \tag{4}$$

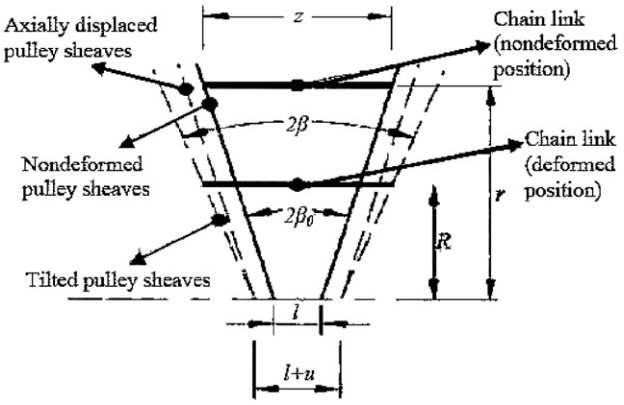

Fig. 4. Pulley deformation model.

2.3. Link–pulley contact description

A chain link contacts a pulley at the ends of a rocker pin. As the plates move, the rocker pins of adjacent links interact with each other. However, assuming negligible dynamic interaction between a pair of rocker pins, the rocker pins are modeled as a single bolt. So, every link is associated with one bolt through which it contacts the pulley sheaves. The bolt dynamics is characterized by a linear massless spring. The surfaces of the bolt are loaded with the normal and frictional contact forces. Fig. 5 illustrates the free body diagram for the interactions between the bolt and a pulley. In this figure, $\mathbf{F}_r$ and $\mathbf{F}_t$ represent the components of the resultant friction force vector $\mathbf{F}_f$ between a chain link and the pulley, which act in the plane of the pulley sheave, and $\mathbf{N}$ is the normal force between the link and the pulley.

It is necessary to quantify the bolt spring force, F_b, in order to derive the contact forces. The bolt force depends on the bolt length l_b and stiffness K_b as well as on the local distance z between the pulley's surfaces. Since the pulley sheaves also bend, additional axial width variation (refer to Fig. 4) affects the bolt force. So, the bolt force, F_b, can be written as

$$F_b = \begin{cases} K_b(l_b - z - u) & \forall (z+u) \leqslant l_b, \\ 0 & \forall (z+u) > l_b. \end{cases} \tag{5}$$

It is to be noted that the chain link slips in the plane of the pulley sheave. The slip angle, γ, defines the plane where the friction force between the chain link and the pulley acts (i.e. γ defines the slip direction). It is the angle which the resultant friction force vector, $\mathbf{F}_f$, makes with a unit tangential direction vector to the pulley. So, in order to get the friction force vector, it is crucial to keep track of the relative velocity vector between the chain link and the pulley. The relative acceleration and the relative velocity between the link and the pulley can be obtained using the contact kinematics depicted in Fig. 6.

2.4. Link–pulley contact-zone friction model

Almost all models, except a few mentioned in the literature, use classical Coulomb–Amonton friction law to model friction between the contacting surfaces of a CVT. The friction phenomenon described by this law is inherently discontinuous in nature. It is common engineering practice to introduce a smoothening function to represent this set-valued friction law. However, certain friction-related phenomena like chaos, limit-cycles, hysteresis, etc., are neither easy to detect nor easy to explain on the basis of classical Coulomb–Amonton friction theory. Since it is difficult to monitor friction experimentally during the running conditions of a complex nonlinear system (e.g. a CVT), mathematical models of friction give insight into the different dynamic maneuvers that a system can undergo.

It is evident that Eqs. (1) and (2) possess time-varying structure due to the possible transitions between stick and slip phases of the contact. However, without significant loss of accuracy [2], it is possible to evade this time-variance in the system by assuming the friction characteristic of the contact zone between the chain link

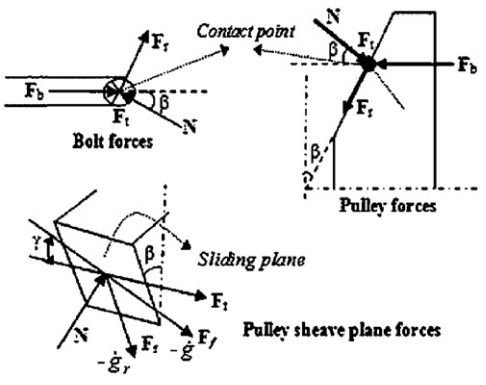

Fig. 5. Link–pulley contact description.

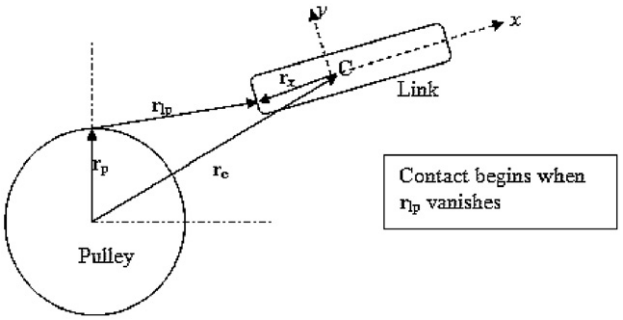

Fig. 6. Link–pulley contact kinematics.

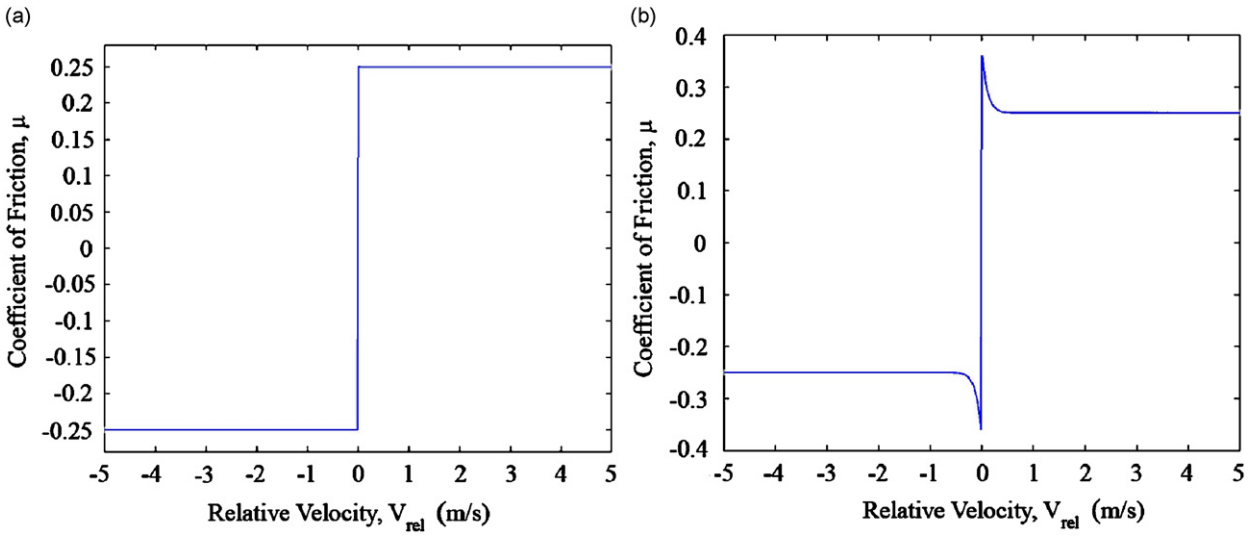

Fig. 7. Friction models for the contact zone: (a) case1: classical Coulomb friction characteristic, μ vs. v_{rel}; and (b) case 2: analytical Stribeck friction characteristic, μ vs. v_{rel}.

and the pulley to be approximated by a smooth nonlinear function. This smooth approximation of the stick-phase of a dry-friction phenomenon obviates the use of event-detection integration methods and linear complementarity problem formulations in a chain CVT model, which consequently leads to time-efficient calculations of the dynamic performance indices. The smoothened system also facilitates the implementation of several tools from nonlinear and chaotic analyses for characterizing the overall behavior and stability of the system. Two different mathematical models are embedded into this planar multibody model of chain CVT in order to capture friction between the link and the pulley under different operating or loading conditions. Fig. 7 depicts the friction characteristics described by these mathematical models. The coefficient of friction between the link and the pulley is governed by the following relationship:

$$case\ 1:\ \mu = a + (\mu_0 - a)(1 - e^{-|v_{rel}|/b}),$$

$$case\ 2:\ \mu = \mu_0(1 - e^{-\kappa|v_{rel}|})(1 + (\sigma - 1)e^{-\chi|v_{rel}|}). \quad (6)$$

The coefficient of friction mentioned in case 1 describes the classical Coulomb–Amonton friction law which aptly captures the dynamics associated with kinetic friction and is most commonly referenced in literature. However, the coefficient of friction mentioned in case 2 is more detailed as it not only captures the dynamics associated with kinetic friction, but also captures the dynamics associated with stiction- and Stribeck-effects (which are prominent under dry and lubricated contact conditions, respectively).

Using continuous (or smooth) friction models and the slip angle, γ, (refer to Fig. 5) the normal force (N or λ_N) on the bolt (or pulley) can be obtained as

$$N(\text{or } \lambda_N) = F_r \tan\beta + \frac{F_b}{\cos\beta},$$

$$F_r = -\mu N \operatorname{sign}(\dot{g}_r) \sin\gamma. \tag{7}$$

Substituting the normal force into Eqs. (4) and (5) yields a solvable system of equations for the generalized coordinates, $\mathbf{q}$, of the chain CVT system.

3. Stick–slip oscillator analogy

Since certain friction characteristics vary continuously with respect to velocity (as in the case of Stribeck friction), friction-driven systems are capable of exhibiting complex and rich nonlinear dynamic behavior such as bifurcations, self-excited vibrations, chaos, etc. Extensive work [25–29] has been done on formulating and understanding the chaotic behavior of 1- and 2-dof systems subjected to friction constraints and periodic forcing functions. Although the exact representation of stick–slip dynamics is based on the theory of differential inclusion [30], it is quite common to use smooth functions to approximate the friction characteristic of the contacting surfaces in relative motion. Although the smoothened system introduces stiff differential equations and may exhibit some drifting behavior (due to the loss of possible limit sets), it plays a significant role in understanding the stick–slip dynamics of a friction-driven system. The subsequently discussed example of a 2-dof stick–slip oscillator highlights the influence of different friction characteristics on the dynamics of the oscillator system. This system not only helps to analyze the richness and complexity of friction-driven dynamics, but also can serve as a paradigm for understanding complex CVT dynamics. Fig. 8 depicts the configuration of the concerned oscillator. The belt moves with a constant velocity and the friction characteristic between the masses and the belt is described by two different mathematical models (refer to Fig. 7). The two interconnected masses over the belt could represent the scenario of two coupled chain links running over a pulley wrap. However, the normal force variation in the CVT system would have a more complex distribution [2,8–12,23] in comparison to the presently discussed stick–slip oscillator system. The equations of motion of the system can be written as

$$\begin{bmatrix} m_1 & 0 \\ 0 & m_2 \end{bmatrix} \begin{Bmatrix} \ddot{x}_1 \\ \ddot{x}_2 \end{Bmatrix} + \begin{bmatrix} c_1 + c_2 & -c_2 \\ -c_2 & c_1 + c_2 \end{bmatrix} \begin{Bmatrix} \dot{x}_1 \\ \dot{x}_2 \end{Bmatrix} + \begin{bmatrix} k_1 + k_2 & -k_2 \\ -k_2 & k_1 + k_2 \end{bmatrix} \begin{Bmatrix} x_1 \\ x_2 \end{Bmatrix} = \begin{Bmatrix} F_1 \\ F_2 \end{Bmatrix},$$

$$\begin{Bmatrix} F_1 \\ F_2 \end{Bmatrix} = \begin{Bmatrix} -\mu m_1 g \operatorname{sgn}|\dot{x}_1 - v| \\ -\mu m_2 g \operatorname{sgn}|\dot{x}_2 - v| \end{Bmatrix}. \tag{8}$$

It is evident from Eq. (8) that a 2-dof stick–slip oscillator has a 4D phase-space representation and also possesses discontinuous right-hand sides (i.e. the forcing vector). Hence, the oscillator represented by Eq. (8) falls under the category of non-smooth mechanical systems, in particular Filippov systems [30]. The non-smooth system in Eq. (8) has two switching boundaries i.e. $\dot{x}_1 = v, \dot{x}_2 = v$. This non-smooth system can be

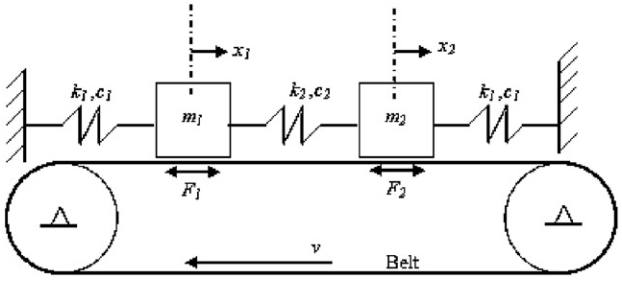

Fig. 8. 2-dof stick–slip oscillator system.

approximated by introducing smoothening functions in the above equation. The smooth approximation of the stick–slip oscillator dynamics is given by

$$\begin{bmatrix} m_1 & 0 \\ 0 & m_2 \end{bmatrix} \begin{Bmatrix} \ddot{x}_1 \\ \ddot{x}_2 \end{Bmatrix} + \begin{bmatrix} c_1 + c_2 & -c_2 \\ -c_2 & c_1 + c_2 \end{bmatrix} \begin{Bmatrix} \dot{x}_1 \\ \dot{x}_2 \end{Bmatrix} + \begin{bmatrix} k_1 + k_2 & -k_2 \\ -k_2 & k_1 + k_2 \end{bmatrix} \begin{Bmatrix} x_1 \\ x_2 \end{Bmatrix} = \begin{Bmatrix} -2\mu m_1 g \tan^{-1}(\lambda(\dot{x}_1 - v))/\pi \\ -2\mu m_2 g \tan^{-1}(\lambda(\dot{x}_2 - v))/\pi \end{Bmatrix}. \tag{9}$$

The smoothened oscillator system, represented by Eq. (9), is examined for various nonlinear phenomena under the influence of two different friction characteristics: (a) constant coefficient of friction (i.e. the classical Coulomb–Amonton friction model, $\mu = \mu_0$), (b) Stribeck friction model i.e. $\mu = \mu_0(1 - e^{-\kappa|v_{rel}|})(1 + (\sigma - 1)e^{-\chi|v_{rel}|})$. The simulation is run for a number of initial conditions i.e. $(\mathbf{x_0}, \dot{\mathbf{x}}_\mathbf{0})$ and the following parameters (in S.I. units), $(k_1, k_2) = 25\,\mathrm{N\,m^{-1}}$; $(c_1, c_2) = 1\,\mathrm{N\,s\,m^{-1}}$; $(m_1, m_2) = 1\,\mathrm{kg}$; $v = 3.5\,\mathrm{ms^{-1}}$; $\mu_0 = 0.25$, $\sigma = 6.5$, $\lambda = 10^4$; $\chi = 1$; $\kappa = 5$; $g = 9.81\,\mathrm{ms^{-2}}$.

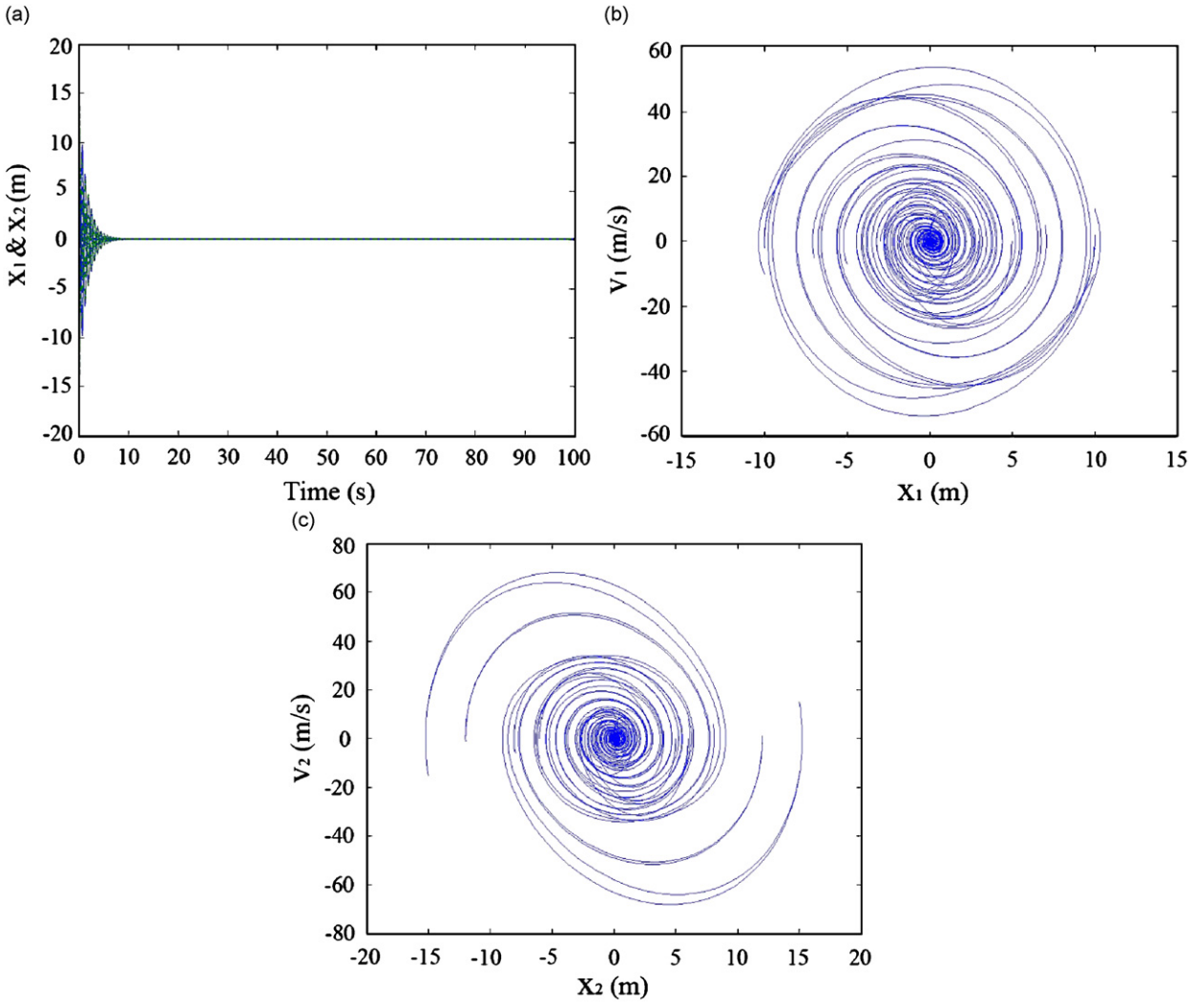

Fig. 9. Dynamic indicators of 2-dof stick–slip oscillator for classical Coulomb friction: (a) displacement time histories of m_1 (x_1, –), m_2 (x_2,- -); (b) phase portrait of m_1; and (c) phase portrait of m_2. Notice the phase trajectories of the system converging to the fixed point.

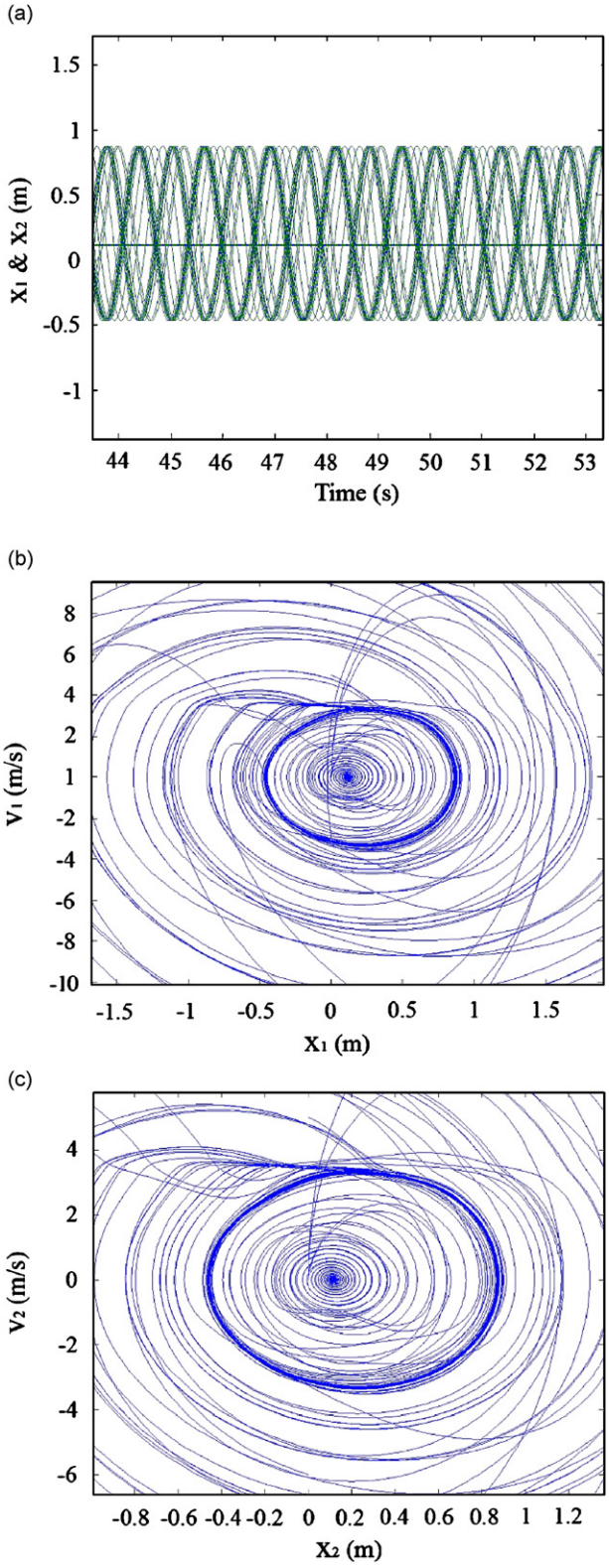

Fig. 10. Dynamic indicators of 2-dof stick–slip oscillator for Stribeck-type friction: (a) displacement time histories of m_1 (x_1, –), m_2 (x_2, - -); (b) phase portrait of m_1; and (c) phase portrait of m_2. Note the presence of an isolated limit cycle in the phase portrait of the system.

Figs. 9 and 10 illustrate the displacement time histories and the phase portraits of the two masses for both cases of friction. It was observed that the system under classical Coulomb–Amonton friction law is always driven towards a stable fixed point for any initial condition. On the other hand, there exists a set of initial conditions for which the same system under the influence of Stribeck friction characteristic exhibits limit-cycle behavior. It can also be noted that the phase trajectories of the system intersect each other for some of the initial conditions. However, these intersections may not necessarily be homoclinic or heteroclinic intersections as the phase-space of the concerned system is multidimensional. The phase portraits in Figs. 9 and 10 are the projections of the time-evolution parameters of the system onto a 2D surface; hence, the intersections in a 2D portrait may represent folding or unfolding of a trajectory in a multidimensional space. Moreover, since Eq. (8) has 4D phase-space representation, it is likely that the system undergoes chaotic behavior. Hence, it is necessary to conduct further analyses on the system to determine whether the system behaves chaotically or not. Figs. 11 and 12 illustrate the Lyapunov exponent spectrum of the smoothened

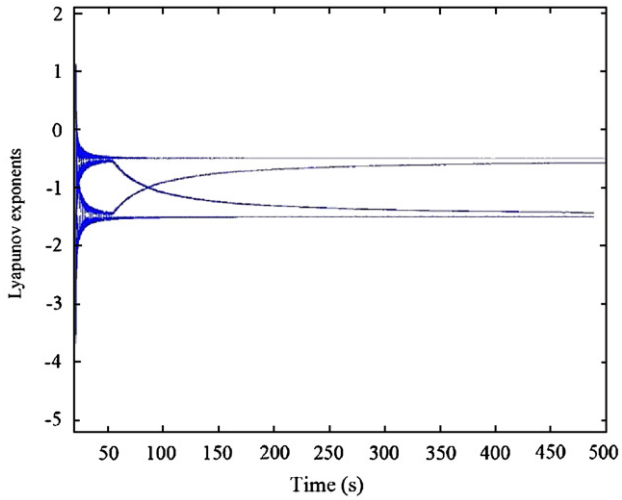

Fig. 11. Lyapunov exponent spectrum of 2-dof stick–slip oscillator under classical Coulomb friction. All Lyapunov exponents of the system are negative, thereby rendering stability into the system.

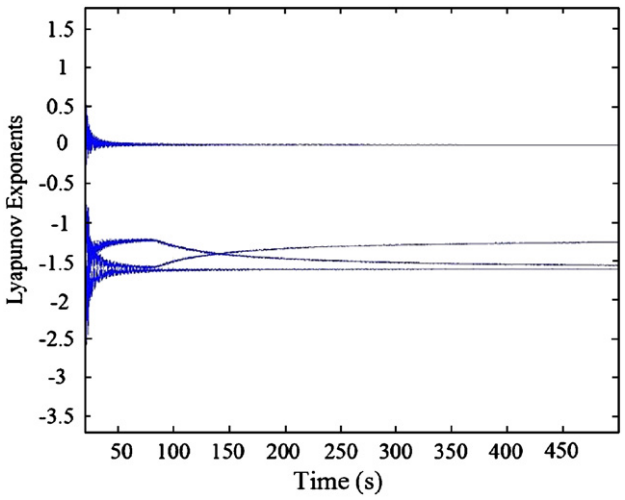

Fig. 12. Lyapunov exponent spectrum of 2-dof stick–slip oscillator under Stribeck-type friction. Note one of the Lyapunov exponents of the system is mildly positive, thereby rendering limit-cycle based mildly chaotic behavior into the system.

stick–slip oscillator system for both cases of friction. For a number of initial conditions close to the basin of attraction, the following Lyapunov exponents were obtained for the system governed by classical Coulomb–Amonton's friction law: (−0.49791 −0.56974 −1.4286 −1.5038). Since all the Lyapunov exponents are negative, the equilibrium point of the system is asymptotically stable, and all the trajectories are attracted towards it. However, as aforementioned, there exists certain set of initial conditions, for instance $[x_1^0, v_1^0, x_2^0, v_2^0] = [0\ 3\ 0\ 6]$, when the system exhibits limit-cycle behavior under the influence of Stribeck friction model. The Lyapunov exponents for the system under Stribeck friction model with the abovementioned initial conditions are found to be: (0.001187 −1.2535 −1.5535 −1.6016). In fact, the system exhibits mild chaos instead of a regular periodic motion as the first Lyapunov exponent is slightly greater than zero. So, the Lyapunov exponent analysis highlights that the apparent limit-cycle behavior of the system under Stribeck friction is not a regular periodic motion, as illustrated by Fig. 10, but a mild chaotic behavior. Thus, the system governed by Stribeck friction not only exhibits regular behavior (as being attracted to a fixed point for certain initial conditions, e.g. [0 0 0 0]), but also can undergo chaos (as for the initial condition of [0 3 0 6]).

4. Results—nonlinear dynamics of chain CVT drives

A chain CVT is a complex nonlinear multibody friction-limited drive whose dynamic performance and torque capacity depend significantly on the friction characteristic of the contacting zone between the chain link and the pulley. Such CVTs are continually subjected to torques from both the engine and the final drive inertias. The engine creates an input torque condition on the driver pulley and the final drive exerts a load torque on the driven pulley. The modeling development was done on the MATLAB/Visual C++ platform. The Runge–Kutta method (with a time-step of 1.0e−6 second) is used to integrate state equations in order to get the time histories of the system states. The simulation of a chain-CVT model starts off with an initial condition of rest and a specific design configuration and computes different dynamic performance indices i.e. axial forces, angular velocities, tension, etc. The driver pulley is subjected to an input torque of 100 N m whereas a low resisting load torque of 50 N m is applied to the driven pulley. The driver and driven pulleys have constant radii of $r_p = 3$ in. (0.0762 m) and $r'_p = 4.5$ in (0.1143 m), respectively. However, the links traverse around the pulley grooves in different pitch radii, thereby, causing a continuous variation in the transmission ratio.

The chain CVT model is subjected to two different friction characteristics (refer to Fig. 7) that describe the friction between the link and the pulley under different operating or loading conditions. Tables 1 and 2 list the numerical values of selected parameters used in the chain CVT simulations.

Figs. 13 and 14 depict the time histories of pulley angular speeds and pulley axial forces, respectively, for both cases. In addition to these time histories, the CVT simulation also outputs other dynamic indices, as reported by Srivastava et al. [8–12]. However, from a controls-design perspective, the nonlinear dynamics and

Table 1
Chain CVT model parameters

Parameters	Values
Non-deformed half sheave angle, β_0	15°
Center distance between pulleys	0.5 m
Mass of a chain link, m	0.1125 kg
Inertia of driver pulley, J_{p1}	1.4516 kg m^2
Inertia of driven pulley, J_{p2}	3.2661 kg m^2
Length of a chain link, L	0.03 m
Bolt stiffness, K_b	200 kN m^{-1}
Bolt length, l_b	0.02 m
Stiffness of force element, k	90 kN m^{-1}
Damping of force element, p	2.7 kN s m^{-1}

Table 2
Parameters for the friction characteristics

	a	b	μ_0	σ	κ	χ
Case 1 (Coulomb)	0.003	0.1	0.25	–	–	–
Case 2 (Stribeck)	–	–	0.25	3.5	10	3

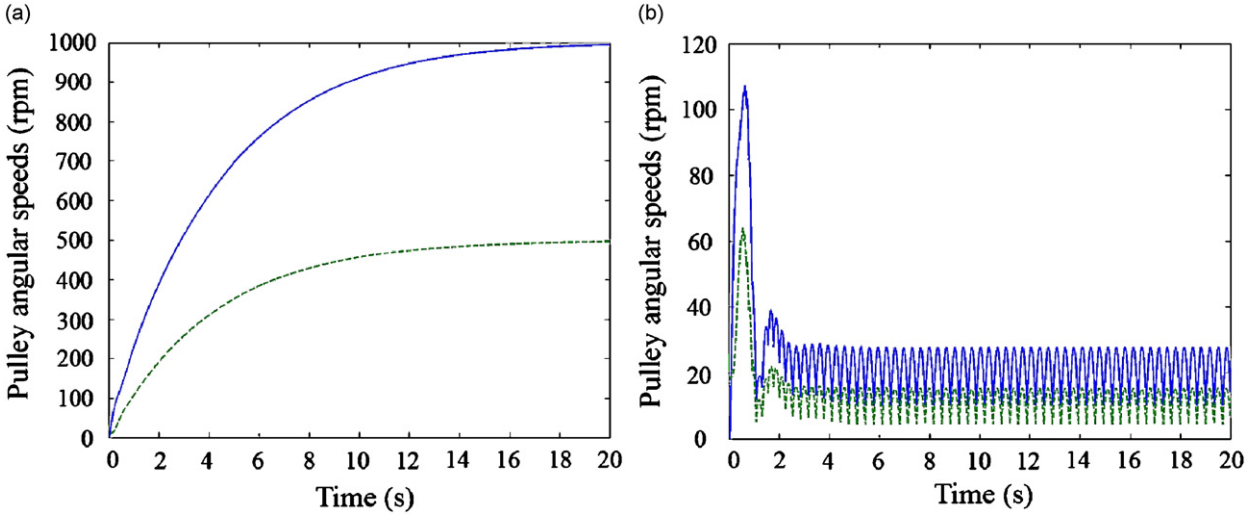

Fig. 13. Time histories of pulley angular speeds at $\tau_{in} = 100\,\text{N m}$ and $\tau_l = 50\,\text{N m}$: (a) CVT under Coulomb friction (driver –, driven - -) and (b) CVT under Stribeck-type friction (driver –, driven - -).

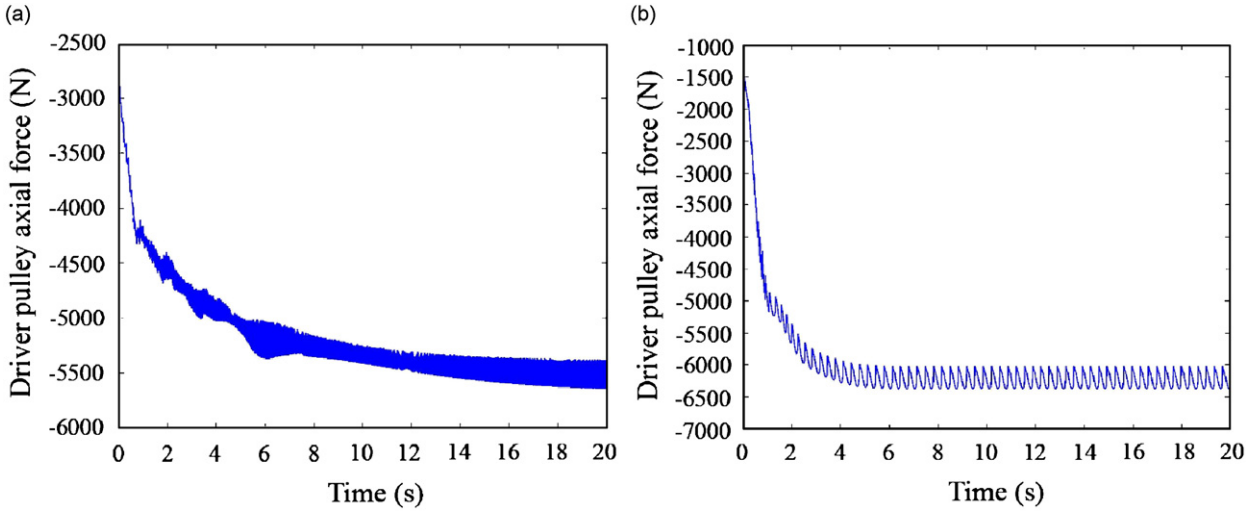

Fig. 14. Time histories of driver pulley axial force at $\tau_{in} = 100\,\text{N m}$ and $\tau_l = 50\,\text{N m}$: (a) CVT under Coulomb friction (i.e. case 1) and (b) CVT under Stribeck-type friction (i.e. case 2).

stability of a chain CVT system could be investigated by analyzing the dynamic performance indices associated with the pulleys (i.e. the pulley axial forces and angular speeds). This could be attributed to the coupling of the pulleys to the engine and final drive inertias. An unstable or irregular behavior in the pulley dynamics is highly likely to influence the dynamics of the engine/final-drive inertia, thereby influencing the overall torque transmission characteristic of the powertrain.

As mentioned previously, the pulleys are subjected to constant torque-loading conditions that arise from the engine and final drive inertias. Hence, under the influence of such constant torque-loads and the friction torques (exerted by the chain links), the pulleys begin to accelerate. It can be inferred from Fig. 13 that the CVT system entails greater losses in case 2 than in case 1 as in spite of a low load torque of 50 N m, it is not able to generate enough friction torque to accelerate the driven pulley faster. Although the transmission losses due to wedging, stiction and Stribeck effects are higher for case 2, there is greater slip loss between the links and pulley for case 1. It is also apparent from the figure that although a CVT system with friction characteristic given by case 2 has lower torque transmitting capacity, its mechanical efficiency (in terms of input-output speed ratios) is comparable to that of a CVT system with case 1 friction characteristic. This can be attributed to the increase in slip losses due to greater radial penetration of the chain links in the pulley grooves under the influence of friction characteristic described by case 1 [8]. Owing to lower torque capacity and higher transmission losses, the pulleys of a CVT system with case 2 friction characteristic also exhibit periodic motions, which could prove to be perilous in the long-run.

Fig. 14 illustrates the time histories of the axial forces on the driver pulley for both cases. Similar trends can be observed for the axial force on the driven pulley sheave. As the chain link moves around the pulleys, it exerts a force in the axial direction on the pulley sheave. The axial force generated along the pulley shaft is computed from the bolt force, as discussed in the earlier section (refer to Eq. (5)). As the local distance between the pulley sheaves varies, the links move radially inwards and outwards within the pulley groove, which causes continuous variations in the transmission ratio. It can be observed from the figure that the axial force required to meet the load torque is higher for a CVT system with Stribeck-type friction characteristic (i.e. in case 2). This can be attributed to the need for a greater transmitted force across the lubricant film in order for the chain links to overcome stiction and hydrodynamic effects and generate friction torques high enough to meet the load requirements on the driven pulley. Moreover, it can also be noted from the figure that the chain links travel much slowly in a CVT system governed by case 2 friction characteristic than by case 1. The large axial force on the pulley sheaves gives rise to undesirable oscillations of the pulley sheaves, which could further induce chaos in the system and lead to early signs of wear. It is apparent from the figure that the pulley sheaves undergo smoother oscillations in the axial direction for case 2 than in case 1. It was evident from the analysis of the 2-dof stick–slip oscillator that for a higher dimensional phase-space, time-histories and phase-portraits of a system are not the sole factors for analyzing its stability. It is necessary to incorporate other tools from nonlinear and chaotic analyses to characterize a system's stability. Hence, further investigation is subsequently done to characterize the nature of the periodic motions associated with the pulley sheaves.

Since it is experimentally cumbersome as well as computationally expensive to record the time histories of each and every state of the CVT system, the most feasible method to analyze the system's stability is to reconstruct its phase space using certain time histories which represent the dynamic performance indices of the system. As mentioned earlier, pulley speeds and axial forces serve as relevant dynamic performance indices (from powertrain controls perspective) for reconstructing the phase space of the CVT system. These time histories, which depend on the states of the CVT system, are sampled at a time interval of 1 ms (i.e. sampling time, $t_s = 0.001$ s) to generate a sequence s_n. The transients are ignored from this sequence of data points and the remaining data (4000 points for the system with case 1 friction characteristic and 10000 points for the system with case 2 friction characteristic) are normalized and later embedded into a higher dimensional phase space using the method of delays.

The method of delays [31] reconstructs the attractor of the original system by generating the vectors, $\mathbf{Y}(n) = [s_n, s_{n+d}, s_{n+2d}, \ldots, s_{n+(m-1)d}]$, where m is the embedding dimension of $\mathbf{Y}(n)$ and d is the embedding delay. Moreover, since the friction characteristics of the contacting components in a CVT system have been approximated by smooth nonlinear functions (refer to Fig. 7), not only the deterministic nature of time series is guaranteed, but also a one-to-one topological mapping between the reconstructed phase space and the real phase space of the system is established by the delay coordinate embedding method. So, the attractor constructed using the aforementioned method of delays will have the same mathematical properties, such as correlation dimension, Lyapunov exponents, recurrence frequencies, etc. as the original system. It is necessary to have a good estimate of both embedding dimension and delay in order to construct a successful or meaningful attractor (i.e. one which can aptly capture or represent the dynamics of the original system).

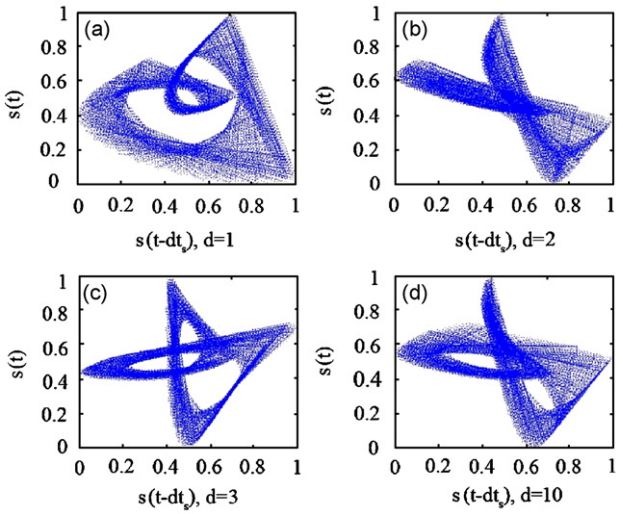

Fig. 15. Time-delayed phase space reconstructions for various embedding delays, d, using driver pulley axial force data for CVT system in case 1 and a sampling time, t_s, of 1 ms: (a) uniform, well-correlated phase-space reconstruction of CVT pulley dynamics using an embedding delay $d = 1$; (b) uncorrelated, skewed phase space reconstruction of CVT pulley dynamics using $d = 2$; (c) slightly complex, uncorrelated, multi-folded phase space reconstruction of CVT pulley dynamics using $d = 3$; and (d) complex, uncorrelated, multi-folded phase space reconstruction of CVT pulley dynamics using $d = 10$. Note $s(t)$ represents the normalized driver pulley axial force data from case 1.

Several methods have been reported in literature to calculate these parameters. For instance, the method of mutual information and the method of false nearest neighbors [32–36] are extensively used to determine the embedding delay and dimension, respectively.

Figs. 15 and 16 illustrate the delay representations for different embedding delays d using the driver pulley axial force time histories for both the cases. It can be observed that with increasing embedding delays, the vectors $\mathbf{Y}(n)$ form increasingly complex structure (especially in case 1) in the reconstructed phase space as their successive elements become almost independent. On the other hand, very small delay causes the vectors to be clustered around the diagonal of the reconstructed phase space, as depicted in Fig. 16(b). Thus, time-delayed representations of the driver pulley axial force in the reconstructed phase space give an apt estimate of the embedding delay needed for conducting further analysis on the behavior of the reconstructed attractor. It is evident from the figures that a unit delay (i.e. $d = 1$) is apt for reconstructing the phase space of the present CVT model in case 1, whereas an embedding delay of 50 (i.e. $d = 50$) is suitable for reconstructing the phase space of the system in case 2. Fig. 17 depicts the optimal embedding dimensions for both cases as obtained by using the algorithm for estimating false nearest neighbors [32] on the sampled data points of the driver pulley axial forces. It can be observed from the figure that the fraction of false nearest neighbors convincingly drops to almost zero for $m = 3$ for case 1 and $m >= 5$ for case 2. This implies that the dynamics corresponding to the motion of pulley sheaves arise from at least a 3D system for case 1 and a 5D system for case 2. It is to be noted that the embedding dimension, here, does not reflect the total number of dof of the system as CVT, being a time-variant structure, experiences continuous wedging, contact-detachment transitions between the links and the pulleys. Hence, the aforementioned embedding dimensions only aim to capture, reconstruct, and analyze the dynamics associated with the motion of pulley sheaves.

Having reconstructed the attractor using these embedding dimensions and delays, one investigates the behavior of these attractors by evaluating the largest Lyapunov exponent of the system as well as by implementing recurrence plotting techniques. Although an m-dimensional system has m Lyapunov exponents, the estimation of the largest Lyapunov exponent is uniquely sufficient to characterize chaos in a system. Lyapunov exponents are related to the exponentially fast divergence and convergence of nearby orbits in phase space, as described by

$$|\delta s(t)| \approx e^{\tilde{\lambda} t} |\delta s(0)| \vee \delta s(0) \to 0, \quad t \to \infty. \tag{10}$$

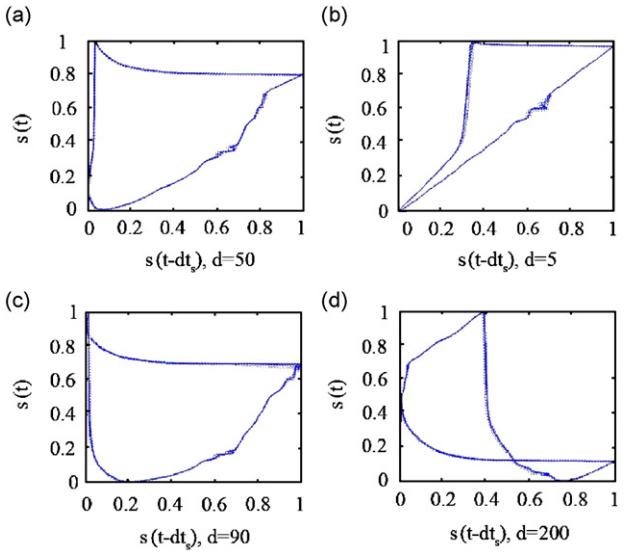

Fig. 16. Time-delayed phase space reconstructions for various embedding delays, d, using driver pulley axial force data for CVT system in case 2 and a sampling time, t_s, of 1 ms: (a) uniform, well-correlated phase-space reconstruction of CVT pulley dynamics using an embedding delay $d = 50$; (b) skewed, tightly correlated phase space reconstruction of CVT pulley dynamics using $d = 5$; (c) uniform, well-correlated phase-space reconstruction of CVT pulley dynamics (with slightly folded edges) using $d = 90$; and (d) slightly complex, uncorrelated phase space reconstruction of CVT pulley dynamics using $d = 200$. Note $s(t)$ represents the normalized driver pulley axial force data from case 2.

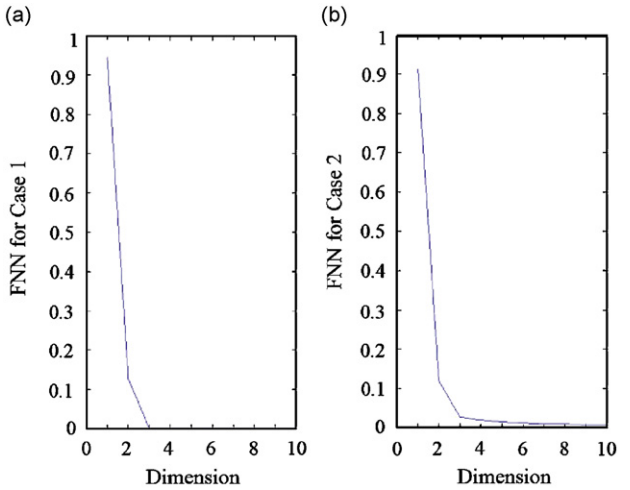

Fig. 17. Determination of minimal embedding dimension using FNN (Fraction of False Nearest Neighbors) algorithm driver pulley axial force data: (a) CVT system with case 1 friction and embedding delay, $d = 1$ and (b) CVT system with case 2 friction and embedding delay, $d = 50$.

A system with one or more positive exponents, $\overline{\lambda}$, is defined to be chaotic. Lyapunov exponents can thus also be considered as analogs to the eigenvalues of a linear system as both of these govern the stability of a system to a large extent. However, the trajectories of chaotic motion do not escape to infinity, but preserve a recurrence property. Several algorithms have been proposed in literature to estimate the Lyapunov spectrum of nonsmooth and smooth mechanical systems [37–39]. Figs. 18 and 19 depict the maximal Lyapunov exponents of the system, which are estimated using the sampled data points of driver pulley axial forces for both cases. The maximal Lyapunov exponents of the attractors were calculated from the algorithms developed

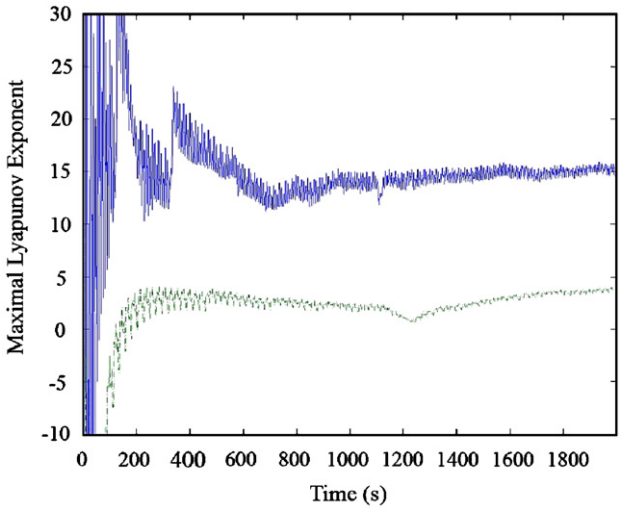

Fig. 18. Maximal Lyapunov exponent for a CVT system under case 1 friction characteristic using driver pulley axial force data: (–: embedding dimension, $m = 3$, embedding delay, $d = 1$, - -: embedding dimension, $m = 10$, embedding delay, $d = 1$).

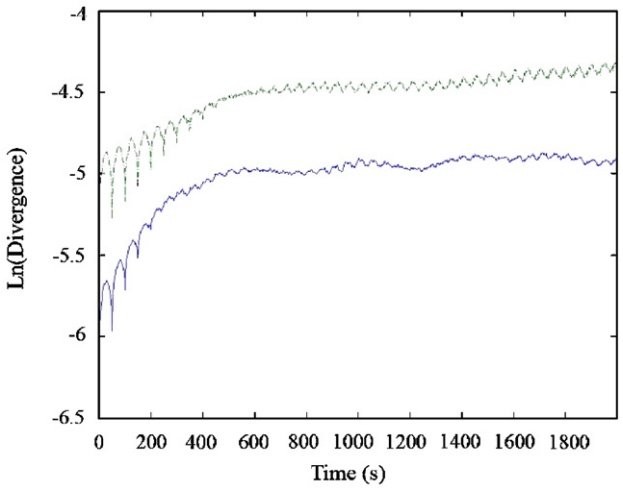

Fig. 19. Divergence of nearby orbits for a CVT system under case 2 friction characteristic using driver pulley axial force data: (–: embedding dimension, $m = 5$, embedding delay, $d = 50$, - -: embedding dimension, $m = 10$, embedding delay, $d = 50$). Slope of this curve estimates the maximal Lyapunov exponent of the system.

by Wolf et al. [37] and by Rosenstein et al. [39] for different combinations of embedding dimensions and embedding delays. It is clear from Fig. 18 that the maximal Lyapunov exponent corresponding to the axial motion of the driver pulley in a CVT system with case 1 friction characteristic is positive, thereby implying chaos in the axial motion of the pulley sheaves. However, it is evident from Fig. 19 that the divergence, which is related to the ratio of separation distances between the trajectories (i.e. $\delta s(t)/\delta s(0)$), for a CVT system with case 2 friction characteristic does not vary significantly with time. The maximal Lyapunov exponent in this case could be readily computed by estimating the variations in the slope of the divergence curve in Fig. 19 with time. Since the variations in the divergence curve are not significant, one would expect the slope to tend to zero with time, thereby implying regular periodicity in the axial motion of the pulley sheaves. However, the system exhibits mild chaos as the slope (or the maximal Lyapunov exponent) is slightly positive. This is further corroborated by observing the evolution of the maximal Lyapunov exponent of the driver pulley angular speed of the CVT system with case 2 friction characteristic (refer to Fig. 20).

In addition to estimating the Lyapunov exponents associated with the motion of the pulleys in a chain CVT system, another powerful diagnostic i.e. recurrence plotting was incorporated to characterize the behavior of these attractors in the reconstructed phase space. Recurrence plot is a 2D square matrix of black and white dots that visualizes when a state in the phase space will recur (the black dots represent the recurrence of a state). A recurrence plot is a record of all the instants when the phase trajectory visits roughly the same area in the phase space. The algorithm works by examining the proximity of every point of the phase trajectory to every other point of the trajectory within a predetermined threshold, say $\overline{\varepsilon}$ ($= 0.01$ for the present analysis). A recurrence plot helps to analyze the dynamics associated with a phase space trajectory by analyzing the long- and small-scale structures of the plot [40]. Figs. 21 and 22 depict the recurrence plots of the CVT system for both cases using the sampled data points of driver pulley axial forces. It is evident from Fig. 21 that the driver pulley of the CVT system in case 1 exhibits chaotic motion as indicated by the presence of randomly

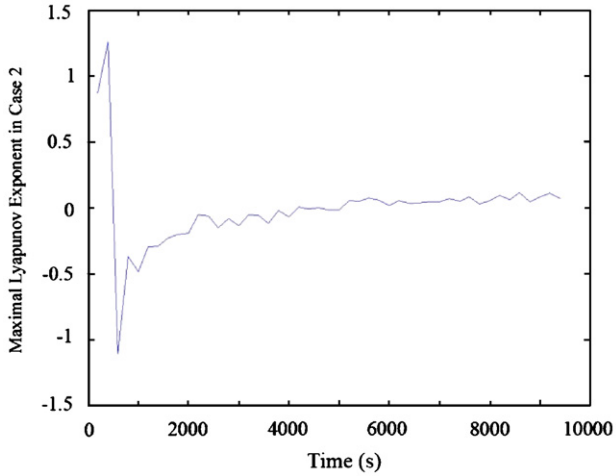

Fig. 20. Maximal Lyapunov exponent of a CVT system under case 2 friction characteristic using driver pulley angular speed data (embedding dimension $m = 5$, embedding delay $d = 50$).

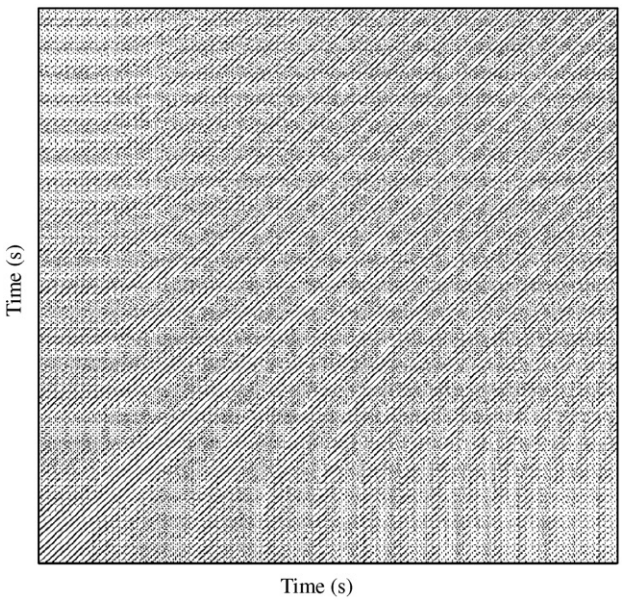

Fig. 21. Recurrence plot of a CVT system under case 1 friction characteristic using driver pulley axial force data.

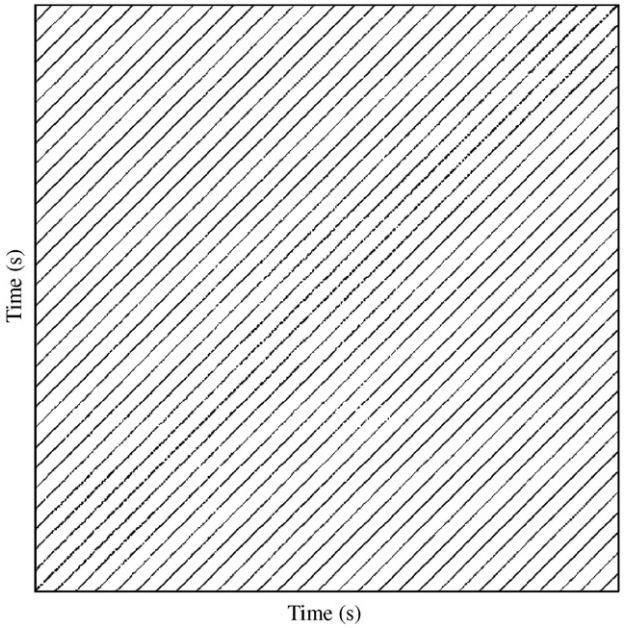

Fig. 22. Recurrence plot of a CVT system under case 2 friction characteristic using driver pulley axial force data.

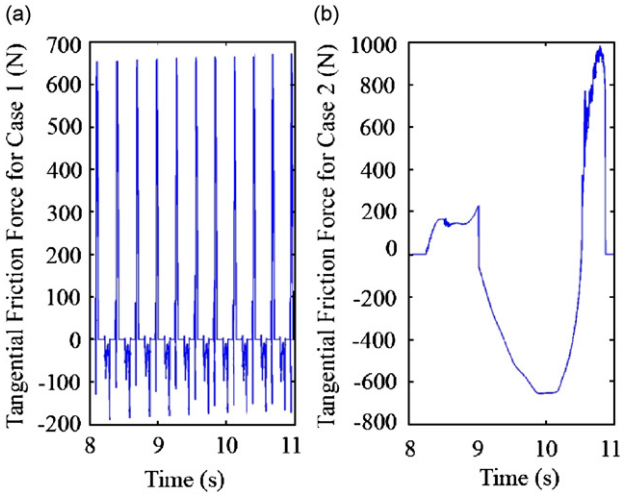

Fig. 23. Time histories of tangential friction force between a chain link and the pulley sheave for a CVT system under: (a) case 1 friction characteristic and (b) case 2 friction characteristic.

distributed diagonal structures among the isolated recurrence points. It is apparent from Fig. 22 that the CVT system under case 2 friction characteristic exhibits regular periodicity because of the presence of smooth parallel diagonal structures. However, closer observation of the figure highlights the presence of certain discontinuities or irregularities in some of the diagonal structures, which consequently induces mild chaos in the dynamics of the pulleys of a chain CVT system. It is interesting to note that although the pulley axial forces exhibit chaotic behavior in both cases, only the pulleys of the chain CVT system with case 2 friction characteristic undergo mildly chaotic angular motion (refer to Fig. 13). This could be attributed to higher stiction and lubrication-related effects in the case of the CVT system with Stribeck-type friction characteristic.

It is evident from the time history of the tangential friction force for both cases in Fig. 23 that the links not only move slower in case 2, but also have to overcome higher stiction and lubrication-related drag (as depicted by the reversal of friction force between 9 and 11 s) to initiate successful torque transmission for meeting the load requirements on the driven pulley. This reversal of friction force due to influence of high stiction and lubrication effects causes periodicity in the angular motion of the pulleys in case 2. However, since the links traverse the pulley wraps faster in case 1, they, in spite of inducing chaos in the axial motion of the pulley sheaves, are able to generate smooth friction torques that consequently yield smoother variations in the angular motion of the pulleys of the CVT system under case 1 friction characteristic. This tangential friction force not only exerts a friction torque on the pulleys, but also acts as a transmitting force responsible for causing variations in the tensile force of the chain links [8]. It can also be noted from Fig. 23 that the transmitting force in case 2 is higher than in case 1. Since chain links traverse greater radial path for a CVT system in case 1 than in case 2, the transmitting force required to overcome the resisting load torque is not high enough for case 1.

5. Conclusions

A chain CVT falls under the category of friction-limited drives and depending on different operating (or loading) conditions and design configurations, the friction characteristic of the contacting components of a CVT may vary. For instance, in case of a fully lubricated CVT, the friction characteristic of the contacting surface may bear a resemblance to the Stribeck curve rather than to a continuous Coulomb characteristic. With an aim to understand friction-induced nonlinear dynamics of a CVT system, two realistic physics-based mathematical models of friction were incorporated in a planar multibody chain CVT model to describe friction between the link and the pulley. These friction characteristics capture the effects not only due to kinetic friction (as in case 1), but also due to stiction and boundary-lubrication (as in case 2).

It was observed that the torque carrying capacity of the CVT system lowered under the presence of friction characteristic described by case 2. Moreover, the chain CVT entails greater losses from noise, vibration, and wedging of the chain links in case 2 than in case 1. The axial force on the pulley sheaves needed to meet the load torque requirements was also observed to be higher for a lubrication-dominated CVT system than for the case of a dry-friction dominated system. It is evident from the results that CVT, being a complex nonlinear system, is capable of exhibiting varied performance under different friction characteristics of the contact zone between the link and the pulley. So, the performance of a CVT can vary drastically from the condition of dry friction to a fully lubricated condition, which was further corroborated by the paradigm of a 2-dof stick–slip oscillator. However, the analogy between the dynamics of a stick–slip oscillator and the CVT system needs to further investigated by incorporating the effects the non-uniform normal force distribution, clearance, time-varying belt velocity, and certain spatial constraints which could account for the traversal of links in and out of the pulley sheaves. Tools from nonlinear dynamics such as Lyapunov exponents, recurrence plotting, phase-space reconstruction, etc., further highlight that a CVT system is capable of exhibiting chaotic vibrations under varying contact-zone friction characteristics. This not only reduces the torque transmitting capacity, but also induces early wear and makes it difficult to be controlled.

A more accurate analysis of the torque transmissibility of a chain CVT system can be done by modeling the links as elastic bodies, accounting for spatial orientation of the chain links (using a spatial model), and by developing a finite element model for elastic deformations in the pulley sheave. However, since the primary goal of this research was to understand the friction-induced nonlinear dynamic behavior of a chain CVT drive, a planar chain CVT with an approximate pulley bending model suffices the purpose. Friction being an inherent non-smooth nonlinearity renders the CVT system non-smooth. Hence, an accurate nonlinear analysis of the behavior and stability of the CVT system could be understood by implementing the tools of non-smooth mechanical systems and differential inclusions. However, from controls design perspective, these smooth nonlinear friction characteristics are able to yield profound insight into the probable behavior exhibited by a CVT system under different operating conditions, thereby enhancing the knowledge-base for designing efficient CVT controllers, analyzing noise and vibration behavior of a CVT-loaded powertrain or vehicle, identifying loss mechanisms, etc. Since an exact knowledge of the friction characteristic in a CVT system can only be obtained by real-time monitoring of the contact patch dynamics in a production CVT, an

experimental investigation is necessary to corroborate the trends associated with the friction-related nonlinear dynamics reported in this paper based on a theoretical model of a chain CVT system. It is also to be noted that the friction model presented in this research is a static-based friction model as the stiction is represented approximately by the conditions of negligible relative velocity. A more accurate analysis of the contact conditions can be done by either using a friction model that accounts for not only the effects of relative velocity, but also the effects of relative acceleration between two contacting surfaces or using linear complementarity formulations. The research reported in this paper emphasizes that not only the dynamic performance and torque capacity of a CVT can reduce in the presence of friction-related nonlinearity, but also the system can exhibit irregular or chaotic behavior that may prove to be perilous to the system with time.

Acknowledgments

This research was supported by the Automotive Research Center (ARC), a US Army TACOM Center of Excellence for Modeling and Simulation of Ground Vehicles. The support and interest of our sponsors is gratefully acknowledged.

References

[1] C. Canudas de Wit, H. Olsson, K.J. Åström, P. Lischinsky, Dynamic friction models and control design, *Proceedings of the 1993 American Control Conference*, San Francisco, California, USA, 1993, pp. 1920–1926.
[2] J. Srnik, F. Pfeiffer, Dynamics of CVT chain drives, *International Journal of Vehicle Design* 22 (1/2) (1999) 54–72.
[3] J. Srnik, F. Pfeiffer, Simulation of a CVT chain drive as a multibody system with variant structure, *Proceedings of the First Joint Conference of International Simulation Societies*, Zurich, Switzerland, 22–25 August 1995, pp. 241–245.
[4] M. Sedlmayr, M. Bullinger, F. Pfeiffer, Spatial dynamics of CVT chain drives, *Proceedings of the CVT 2002 Congress*, VDI-Berichte, 1709, Düsseldorf, Germany, October 2002, pp. 511–552.
[5] F. Pfeiffer, M. Sedlmayr, Force reduction in CVT chains, *International Journal of Vehicle Design* 32 (3/4) (2003) 290–303.
[6] H. Sattler, Efficiency of metal chain and V-belt CVT, *Proceedings of the International Congress on Continuously Variable Power Transmission CVT 99*, Eindhoven, The Netherlands, 16–17 September 1999, pp. 99–104.
[7] P. Tenberge, Efficiency of chain CVTs at constant and variable ratio: a new mathematical model for a very fast calculation of chain forces, clamping forces, clamping ratio, slip, and efficiency, *2004 International Continuously Variable and Hybrid Transmission Congress*, Paper no. 04CVT-35, San Francisco, USA, 23–25 September 2004.
[8] N. Srivastava, I. Haque, Influence of friction characteristic on the performance of chain CVT drives, *Journal of KONES Powertrain and Transport* 13 (2) (2006) 405–419.
[9] N. Srivastava, Y. Miao, I. Haque, Influence of clearance on the dynamics of chain CVT drives, *2006 ASME International Mechanical Engineering Congress*, Paper no. IMECE2006-14059, Chicago, IL, USA, 5–10 November 2006.
[10] N. Srivastava, I. Haque, Clearance and friction induced dynamics of chain CVT drives, *Multibody System Dynamics* 19 (3) (2008) 255–280.
[11] N. Srivastava, I. Haque, Clearance-induced nonlinear dynamics of chain CVT drives, *2007 International Congress on Continuously Variable and Hybrid Transmissions*, Paper no. 104 (20074545), Yokohama, Japan, 12–14 September 2007, pp. 19–24.
[12] N. Srivastava, I. Haque, Dynamics of chain CVT drives: effects of friction characteristic, *2007 ASME International Design Engineering Technical Conferences*, IDETC/CIE 2007, Paper no. DETC2007-35575, Las Vegas, Nevada, USA, 4–7 September 2007.
[13] W. Lebrecht, F. Pfeiffer, H. Ulbrich, Analysis of self-induced vibrations in a pushing V-belt CVT, *2004 International Continuously Variable and Hybrid Transmission Congress*, Paper no. 04CVT-32, San Francisco, USA, 23–25 September 2004.
[14] J.D. Micklem, D.K. Longmore, C.R. Burrows, Modelling of the steel pushing V-belt continuously variable transmission, *Proceedings of the Institution of Mechanical Engineers, Part C: Journal of Mechanical Engineering Science* 208 (1994) 13–27.
[15] G. Carbone, L. Mangialardi, G. Mantriota, EHL visco-plastic friction model in CVT shifting behaviour, *International Journal of Vehicle Design* 32 (3/4) (2003) 333–357.
[16] N. Srivastava, I. Haque, On the transient dynamics of a metal pushing V-belt CVT at high speeds, *International Journal of Vehicle Design* 37 (1) (2005) 46–66.
[17] N. Srivastava, I.U. Haque, On the operating regime of a metal pushing V-belt CVT under steady state microslip conditions, *2004 International Continuously Variable and Hybrid Transmission Congress*, Paper no. 2004-34-2851 (04CVT-11), San Francisco, USA, 23–25 September 2004.
[18] N. Srivastava, V.Y. Blouin, I.U. Haque, Using genetic algorithms to identify initial operating conditions for a transient CVT model, *2004 ASME International Mechanical Engineering Congress*, Paper no. IMECE2004-61999, Anaheim, CA, USA, 13–19 November 2004.
[19] N. Srivastava, I. Haque, Transient dynamics of metal V-belt CVT: effects of pulley flexibility and friction characteristic, *ASME Journal of Computational and Nonlinear Dynamics* 2 (1) (2007) 86–97.

[20] N. Srivastava, I. Haque, Transient dynamics of metal V-belt CVT: effects of band pack slip and friction characteristic, *Mechanism and Machine Theory* 43 (4) (2008) 459–479.
[21] F. Pfeiffer, C. Glocker, *Multibody Dynamics with Unilateral Contacts*, Wiley-Interscience, New York, USA, 1996.
[22] F. Sorge, Influence of pulley bending on metal V-belt mechanics, *Proceedings of the International Conference on Continuously Variable Power Transmission*, Japanese Society of Automotive Engineers, Paper no. 102 (9636268), Yokohama, Japan, 11–12 September 1996, pp. 9–15.
[23] G. Carbone, L. Mangialardi, G. Mantriota, The influence of pulley deformations on the shifting mechanism of metal belt CVT, *ASME Journal of Mechanical Design* 127 (2005) 103–113.
[24] D. Sferra, E. Pennestri, P.P. Valentini, F. Baldascini, Dynamic simulation of a metal-belt CVT under transient conditions, *Proceedings of the DETC02, 2002 ASME Design Engineering Technical Conference*, Paper no. DETC02/MECH-34228, Vol. 5A, Montreal, Canada, September 29–October 2, 2002, pp. 261–268.
[25] H. Dankowicz, A.B. Nordmark, On the origin and bifurcations of stick–slip oscillations, *Physica D* 136 (3) (2000) 280–302.
[26] P. Stelter, W. Sextro, Bifurcations in dynamical systems with dry friction, *International Series of Numerical Mathematics* 97 (1991) 343–347.
[27] R.A. Ibrahim, Friction-induced vibration, chatter, squeal, and chaos—part II: modeling and dynamics, *ASME Applied Mechanics Reviews* 47 (7) (1994) 227–253.
[28] J. Awrejcewicz, J. Delfs, Dynamics of a self-excited stick–slip oscillator with two-degrees-of-freedom—part II: slip–stick, slip–slip, stick–slip transitions, periodic and chaotic orbits, *European Journal of Mechanics A: Solids* 9 (5) (1990) 397–418.
[29] U. Galvanetto, Bifurcations and chaos in a four-dimensional mechanical system with dry friction, *Journal of Sound and Vibration* 204 (4) (1997) 690–695.
[30] A.F. Filippov, *Differential Equations with Discontinuous Right-hand Sides*, Kluwer Academic Publishers, Dordrecht, The Netherlands, 1988.
[31] H. Kantz, T. Schreiber, *Nonlinear Time Series Analysis*, Cambridge University Press, Cambridge, UK, 1997.
[32] S. Kodba, M. Perc, M. Marhl, Detecting chaos from a time series, *European Journal of Physics* 26 (2005) 205–215.
[33] M. Kennel, R. Brown, H.D.I. Abarbanel, Determining embedding dimension for phase-space reconstruction using a geometrical construction, *Physical Review A* 45 (1992) 3403–3411.
[34] A.M. Fraser, H.L. Swinney, Independent coordinates for strange attractors from mutual information, *Physical Review A* 33 (2) (1986) 1134–1140.
[35] B.F. Feeny, J.W. Liang, Phase-space reconstructions of stick–slip systems, *Proceedings of the ASME 1995 Design Engineering Technical Conferences*, 3A, ASME DE-Vol. 84-1, Long Beach, California, USA, September 1995, pp. 1061–1070.
[36] A.M. Fraser, Reconstructing attractors from scalar time series: a comparison of singular system analysis and redundancy criteria, *Physica D* 34 (1989) 391–404.
[37] A. Wolf, J.B. Swift, H.L. Swinney, J.A. Vastano, Determining Lyapunov exponents from a time series, *Physica D* 16 (1985) 285–317.
[38] P.C. Müller, Calculation of Lyapunov exponents for dynamic systems with discontinuities, *Chaos, Solitons and Fractals* 5 (9) (1995) 1671–1681.
[39] M.T. Rosenstein, J.J. Collins, C.J. De Luca, A practical method for calculating largest Lyapunov exponents from small data sets, *Physica D* 65 (1–2) (1993) 117–134.
[40] J.-P. Eckmann, S.O. Kamphorst, D. Ruelle, Recurrence plots of dynamical systems, *Europhysics Letters* 4 (9) (1987) 973–977.